INTERNATIONAL JOURNAL OF PRECISION ENGINEERING AND MANUFACTURING Vol. 16, No. 3, pp. 479-485 MARCH 2015 / 479
DOI: 10.1007/s12541-015-0065-6

# Design and Optimization of Long Stroke Planar Motion Maglev Stage using Copper Strip Array

**Siwoong Woo[1] and Dae-Gab Gweon[2,#]**

1 Department of Mechanical Engineering, KAIST, 291 Daehak-ro, Yuseong-gu, Daejeon, 305-701, South Korea
# Corresponding Author / E-mail: dggweon@kaist.ac.kr, TEL: +82-42-350-3225, FAX: +82-42-350-5225

KEYWORDS: Maglev, Planar motion stage, Long stroke stage, Precision stage, Magnetic levitation stage

*The main purpose of this proposed maglev stage is to transport a 450 mm wafer in a vacuum environment. To realize a long stroke and a large size mover, a stator was designed using a copper strip array. The mover contains a halbach magnet array and the fixture part has characteristics of low weight and high structural bandwidth for fast response. Since the relationship between the design variables and the system performance is complicated, an optimization procedure was used to obtain optimal design variables. Based on the optimization solution, detailed design was performed and the system's stability was checked by several simulations. Finally, the proposed maglev system was manufactured.*

Manuscript received: August 5, 2014 / Revised: November 13, 2014 / Accepted: November 22, 2014

## 1. Introduction

The stage system for semiconductor lithography or inspection requires the highest performance. Recently, a larger wafer size and a new light source for optical lithography are two important issues in the semiconductor industry. To expose a larger size wafer, the motion range of the stage should become longer. In addition, the stage should move quickly with high velocity and high acceleration, since manufacturing the throughput is closely related to how quickly the wafer stage can move. If EUV is used as a light source for optical lithography, the environment should be a high vacuum. The magnetic levitation stage is suitable to achieve long range and high speed in a vacuum environment. One way to deal with the vacuum environment is to use magnetic levitation, which employs non-contact and non-outgas actuators and guides. Moreover, if the actuators are composed as a planar motor, long range and high speed motion can be realized because of a single moving body with fast response.

Kim first developed six d.o.f magnetic levitation motors using four linear motors.[1,2] One unit is made up of a three phase coil set and a halbach magnet array. This unit generates both the levitation and thrust forces. This planar motor has a very short stroke of 50mm X 50mm in a XY plane because each magnet array should stay above its own unit. Ueda and Ohsaki proposed planar motors using a 2D magnet array with multi-layered long coils in order to increase the rage of motion.[3-5] This planar motor has perpendicular layers of coils. One layer generates force in the y-and z-directions by passing current through the x-direction. The other layer generates force in the x-and z-directions. The magnetic flux density that each coil array feels decreases exponentially. The effectiveness of coils is also poor because the part under the magnet is only used to generate force. Planar motors using magnet – square coil topology have also been developed.[6-8] It consists of a NS-magnet array and a square-shape coil array to levitate and propel the mover. Four coils compose one set and each set generates a force vector in the xyz-plane on the mover. Four groups are able to control six degrees-of-freedom motion. However, the force coupling between the x-and y-directions makes control complex and difficult. The planar motors developed by Philips Applied Technology[9] and by Jansen[10,11] consist of a 2D halbach magnet array and rectangular shape coils. It is a very strong advantage that the force components in x-and y-directions are decoupled, due to coils rotated 45 degrees with respect to the magnet array compared to the square coil array. X. Lu developed 6D direct-drive planar motion stage.[12] That system is an improved version of Kim's system and Ueda's system. The stator is manufactured by a multi layered PCB instead of a coil array and a motion range is expanded. However, the motion range and mover size are still not enough to be used in the semiconductor industry.

This paper proposes a long stroke planar motion maglev stage using a copper strip array that has 450 mm motion range and 500 mm mover size. To maximize the force of the proposed system, an analytical modeling of magnetic force and an optimization procedure were

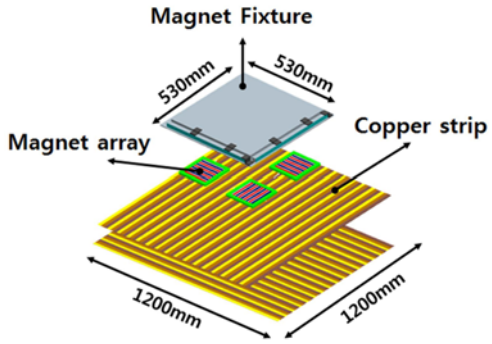


Fig. 1 Schematic of proposed system

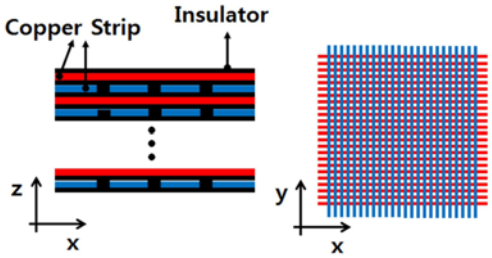


Fig. 2 Schematic of stator using copper strip

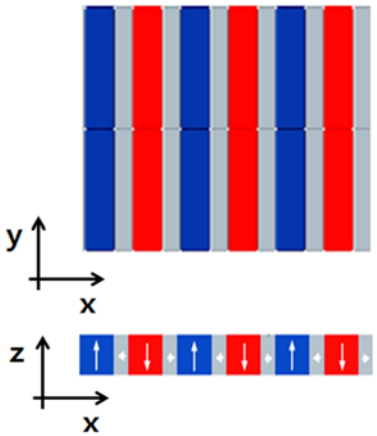


Fig. 3 Schematic of halbach magnet array

executed. Before manufacturing the proposed system, a system's safety was confirmed by modal analysis and thermal simulation.

## 2. Conceptual Design of the Proposed System

Fig. 1 shows the schematic of the proposed system. A stator is made with layers of copper strip array. The structure of the copper strip can decrease the difference between two thrust forces and the resistance of the conductor because of the high aspect ratio. The magnet set is made up of a halbach magnet array to improve the magnetic flux density. The combination of four sets of magnet and layers of copper strip array can generate six d.o.f forces and torques.

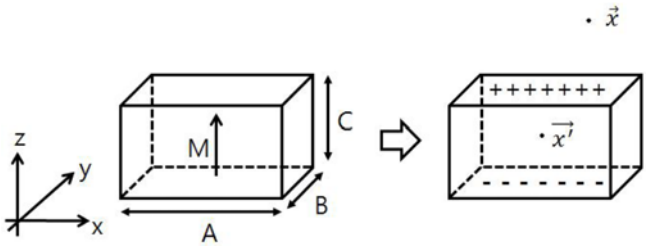


Fig. 4 Concept of surface charge model

## 3. Analytical Modeling of the Magnetic Force

Lorentz force is generated when a current passing coil is placed in the magnetic field.[13] The force $\vec{F}$ is obtained by the following equation:

$$\vec{F} = \int_{coil} id\vec{l} \times \vec{B} \tag{1}$$

where, $l$ is the length of the coil and $\vec{B}$ is the external magnetic flux density. In order to obtain a high force, it is obvious that a high magnetic flux density, long coil and high current are favorable. But these factors are also related to the moving mass, heat generation from ohmic loss, and power consumption. To obtain the optimal performance, an optimization procedure is an essential process.

In order to optimize the force, a magnetic flux and a Lorentz force model must be established. Several methods to calculate the magnetic flux have been developed such as the magnetic nodes method,[14] the surface current method,[13] and the surface charge method.[13] In this paper, the surface charge method was used since it is accurate. In this method, a magnet was expressed to a distribution of equivalent charges. Fig. 4 shows the magnet that is magnetized in the positive z-direction.

Magnetic flux was obtained by the following integral equation:[13]

$$B(x) = \frac{1}{4\pi}\int_V \frac{\nabla' \cdot M(x')}{|x-x'|}dv' - \frac{1}{4\pi}\int_S \frac{M(x') \cdot \hat{n}}{|x-x'|}ds' \tag{2}$$

where $x$ is the observation point, $x$' is the source point, $S$ is the surface that bonds $V$, and n is the outward unit normal to $S$. The solutions of Eq. (1) in rectangular coordinates are given by Eq. (2)~(4).[15]

$$B_x = \frac{B_r}{4\pi}\Sigma_{i=0}^{1}\Sigma_{j=0}^{1}\Sigma_{k=0}^{1}(-1)^{i+j+k}\log(R-T) \tag{3}$$

$$B_y = \frac{B_r}{4\pi}\Sigma_{i=0}^{1}\Sigma_{j=0}^{1}\Sigma_{k=0}^{1}(-1)^{i+j+k}\log(R-S) \tag{4}$$

$$B_z = \frac{B_r}{4\pi}\Sigma_{i=0}^{1}\Sigma_{j=0}^{1}\Sigma_{k=0}^{1}(-1)^{i+j+k}\mathrm{atan}\left(\frac{ST}{RU}\right) \tag{5}$$

Where, $R = \sqrt{S^2+T^2+U^2}$

$$S = (x-x') - (-1)^i A/2$$

$$T = (y-y') - (-1)^j B/2$$

$$U = (z-z') - (-1)^k C/2$$

The above model has z-directional magnetization. In order to analyze


Fig. 5 Concept of image method

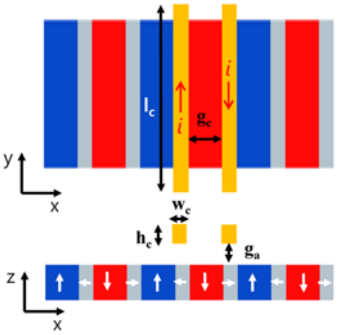


Fig. 6 Comparison model of analytical modeling and FEM

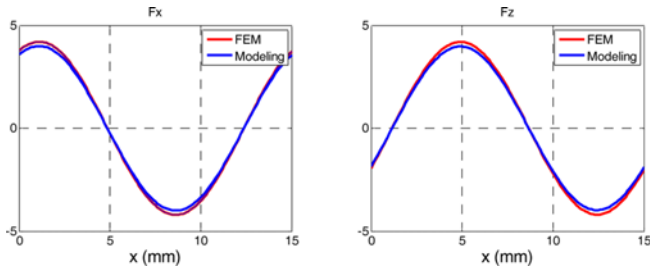


Fig. 7 Comparison results of analytical modeling and FEM

a halbach magnet array containing magnet blocks, which are placed on the other position with different magnetization directions, magnetic flux should be calculated by transforming the coordinate.

In the proposed system, iron back yokes are used to help assemble the magnet array and to increase magnetic flux. The method of images is used to solve field problems when the source is near a material with high permeability, and the solution region manifests a high degree of symmetry.[13] Fig. 5 shows the concept of the method of image.

The Lorentz force can be obtained using the previous magnetic flux model. Fig. 6 shows a halbach magnet array and conductors. The Lorentz force can be obtained by Eqs. (6) and (7) in this model.

$$F_x = j\int_0^{l_c}\int_0^{w_c}\int_{g_a}^{g_a+h_c} B_z dzdxdy - j\int_0^{l_c}\int_{g_c+w_c}^{g_c+2w_c}\int_{g_a}^{g_a+h_c} B_z dzdxdy \quad (6)$$

$$F_z = j\int_0^{l_c}\int_0^{w_c}\int_{g_a}^{g_a+h_c} B_x dzdxdy - j\int_0^{l_c}\int_{g_c+w_c}^{g_c+2w_c}\int_{g_a}^{g_a+h_c} B_x dzdxdy \quad (7)$$

The results of analytical modeling and FEM were compared to verify the accuracy of analytical modeling. When the magnet array moved in the x-direction, the magnetic forces were obtained. Fig. 7 and Table 1 show the results of comparison. The results show that the analytical modeling and FEM are highly similar. The maximum difference is just 5.26%.

Table 1 Comparison results of analytical modeling and FEM

| | Thrust force (Fx) | | Levitation force (Fz) | |
|---|---|---|---|---|
| | Peak value | RMS value | Peak value | RMS value |
| Modeling (N) | 3.996 | 2.826 | 3.973 | 2.809 |
| FEM (N) | 4.206 | 2.974 | 4.193 | 2.965 |
| Error (%) | 4.99 | 4.98 | 5.25 | 5.26 |

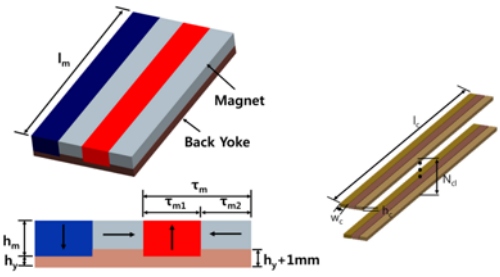


Fig. 8 Design parameters for proposed system

Table 2 Design parameters for proposed system

| Description | Design variable | Unit |
|---|---|---|
| Thickness of magnet array | $h_m$ | mm |
| Halbach ratio | $\eta$ | - |
| No. of layers | $N_c$ | - |
| Description | Fixed parameter | Unit |
| Length of strip | $l_c = 1000$ | mm |
| Width of strip | $w_c = 5$ | mm |
| Thickness of strip | $h_c = 0.07$ | mm |
| Length of magnet array | $l_m = 260$ | mm |
| Description | Dependent parameter | Unit |
| Thickness of yoke | $h_y = h_m/2$ | mm |
| Pole pitch of magnet array | $\tau_m = 3w_c$ | mm |
| Width of main magnet | $\tau_{m1} = \eta \times \tau_m$ | mm |
| Width of intermediate magnet | $\tau_{m2} = (1-\eta) \times \tau_m$ | mm |

## 4. Optimal Design

There are so many design parameters and these parameters are related to force and moving mass. Before the optimization procedure, the parameters were classified into three categories: Design variables, relative parameters and fixed parameters.

The design variables are related to the force and the moving mass which are the thickness of magnet array (hm), the halbach ratio ($\eta$) and the number of strip layers (Ncl). The fixed parameters were determined by a machinability of materials, which are required equipment. The relative parameters are related to the design variables and the fixed parameters.

Fig 8 represents the design parameters of the maglev system. The parameters are shown in Table 2.

The purpose of optimization is to maximize the magnetic force per mover mass. For the optimal design variables, a sequential quadratic programming (SQP)[16] method was used. Doing so can result in high acceleration and control performance. The following objective function was used:

$$\text{Minimize}\left(\frac{M}{F}\right) \quad (8)$$

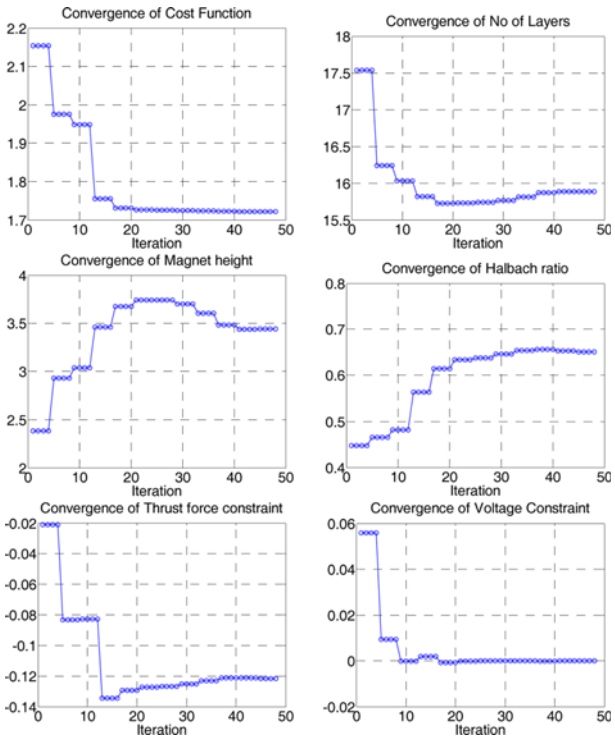


Fig. 9 Convergence of cost function, design variables and constrants

where, M is the mass of the mover and F is the thrust force. The optimization problem includes a number of constraints to achieve target performance and to prevent the overload of the system. There are three constraints in this optimization procedure. The first constraint is related to the levitation force. To levitate the mover in the stage system, levitation force should exceed at least Mg. Four magnet array sets can generate levitation force. Each magnet array set has to generate Mg/4. The thrust force should also be considered. When target acceleration is $a_{max}$, each magnet array set has to generate $Ma_{max}/2$. Because the thrust forces are generated in both directions, two magnet array sets accelerate in the x-direction and others in the y-direction. Lastly, the voltage and current specification should be matched with the amplifier. The required maximum voltage and current should be under an allowable voltage and the current of the amplifier should be at maximum velocity and acceleration. The maximum voltage at maximum velocity and acceleration is given by

$$\text{Max. Voltage} = i_{max}R + K_{EMF}v_{max} \tag{9}$$

where, $i_{max}$ is the maximum current, R is the resistance of the copper strip, $K_{EMF}$ is the back EMF constant, and $v_{max}$ is the maximum velocity.

The converged cost function, design variable, and constraint are shown in Fig. 9. The SQP method does not guarantee a global minimum. To guarantee the global minimum, seven optimization procedures were performed with different random initial points. The results of the repeated optimization procedure are given in Table 3. All the optimization results are converged to one constant value. Statistically, the global minimum is founded according to the Bayesian stopping rule,[17] given by

$$w\frac{n-1}{n-w-2}-\frac{1}{2}\le w \tag{10}$$

where, n is the number of optimizations and w is the number of local minimums.

Table 3 Optimization results

| Initial parameters | | | Optimized parameter | | | |
|---|---|---|---|---|---|---|
| $h_m$ | ç | $N_{cl}$ | $h_m$ | ç | $N_{cl}$ | Cost |
| 2.3858 | 4.4779 | 17.5364 | 3.4391 | 6.4288 | 15.8836 | 1.7219 |
| 5.8245 | 7.3008 | 10.4782 | 3.4399 | 6.4262 | 15.8823 | 1.7219 |
| 2.9391 | 6.4126 | 16.596 | 3.4395 | 6.4234 | 15.8838 | 1.7219 |
| 3.4770 | 5.4448 | 16.2420 | 3.4389 | 6.4287 | 15.8837 | 1.7219 |
| 3.9570 | 6.3509 | 17.2004 | 3.4383 | 6.4297 | 15.8847 | 1.7219 |
| 2.1378 | 6.7550 | 14.9078 | 3.4394 | 6.4291 | 15.8835 | 1.7219 |
| 3.9591 | 6.7823 | 16.2316 | 3.4369 | 6.4299 | 15.8851 | 1.7219 |

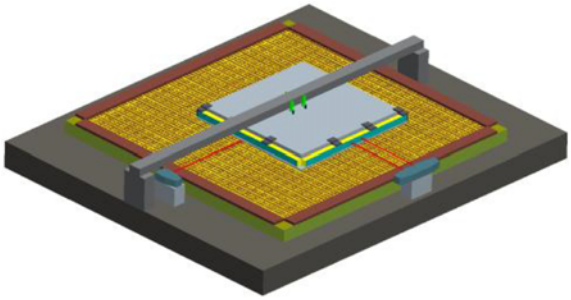

Fig. 10 3D model for proposed system

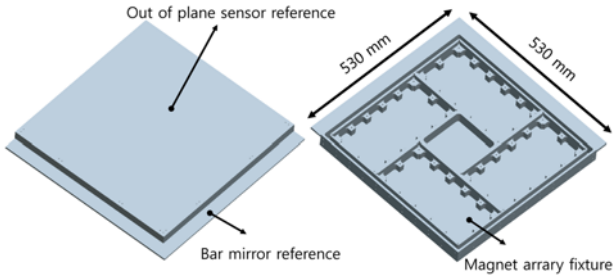


Fig. 11 3D model for fixture part

## 5. Realization of the Proposed System

In this section, the realized system is presented. Fig. 10 shows a 3D model of the proposed system.

The mover is made up of a fixture part, four magnet arrays, and two bar mirrors. The roles of the fixture part are not only fixing magnet arrays, but also referring sensors. To minimize the assembly error, the fixture part is machined into monolithic construction. Fig. 11 shows a 3D model of the fixture part.

Magnets are fixed on a steel back yoke and these amgnets are surrounded by a polymer guide. Fig. 12 shows a 3D assembly drawing of the magnet array set. Four magnet array sets are fixed at the under surface of the fixture part and two bar mirrors are mounted on the upper edge surface.

A modal analysis is necessary to check the allowable control bandwidth and robustness against dynamic disturbances. The results of

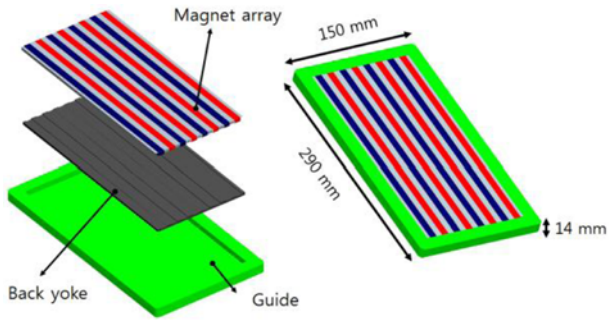


Fig. 12 3D model for magnet array

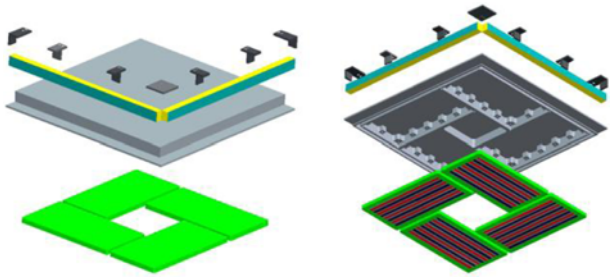

Fig. 13 3D model for mover

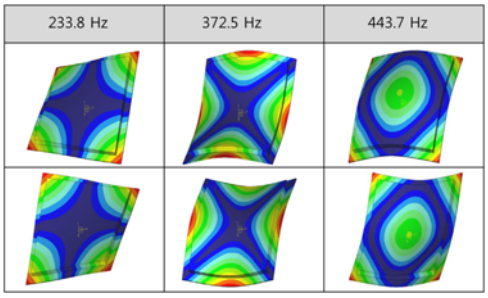


Fig. 14 Results of modal analysis

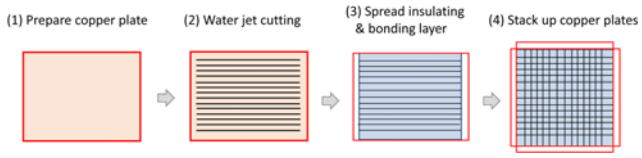


Fig. 15 Manufacturing sequence of copper strip array

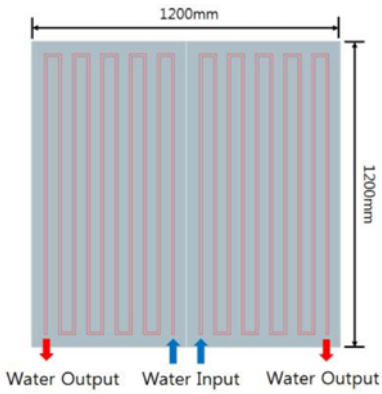


Fig. 16 Coolant circulation channel plate

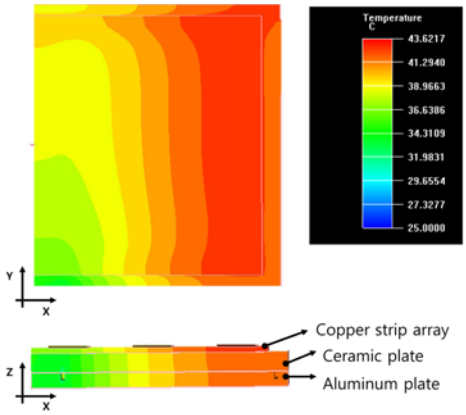


Fig. 17 Heat simulation result

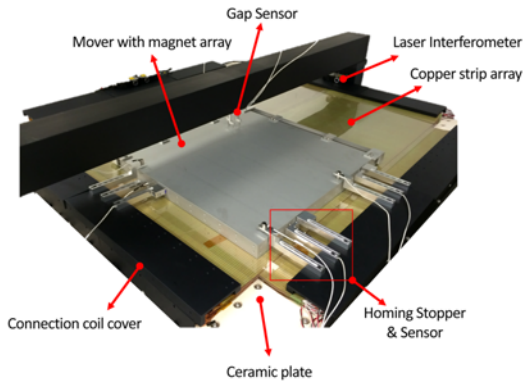


Fig. 18 Manufactured maglev system

modal analysis show that the control bandwidth should be below 250 Hz and the disturbance rejection should be indispensable over the first mode.

To manufacture the strip arrays, copper thin plates need to be prepared. After water jet cutting, each plate is coated into insulating and bonding layers. Finally, worked plates are stacked up perpendicularly.

A heat exchanger with coolant is located right below the strip arrays. Two channels are engraved on the bottom surface. The channels are closed by a ceramic plate on which the strip arrays are located. The ceramic material was chosen to have high thermal conductivity for the heat transfer and low electric conductivity was chosen for the prevention of an eddy current. The coolant circulates through each channel and the heat from the strips is transferred to the coolant.

The heat transfer from the strip arrays to the water coolant was simulated using Ansys Icepak 4.0. Only half of the system was considered because of the bilateral symmetry. Strip arrays were considered as a heating source. The maximum heat generation of 1400 W is exerted on strip arrays. The water flow rate from the chilling

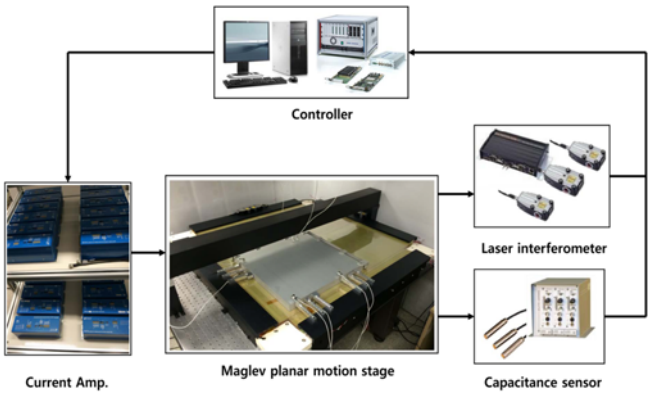


Fig. 19 Schematic diagram of the hardware setup

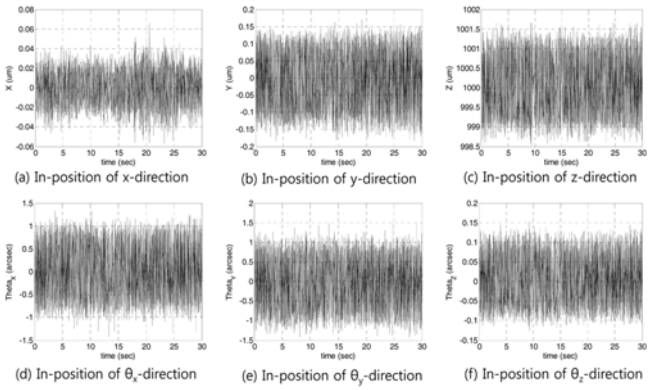


Fig. 20 In-position stability

circulator was 0.6 L/min and the initial water temperature was 25°C. Fig. 17 shows the simulation results that the strip arrays, ceramic plate, and aluminum plate have temperatures below 45°C.

The proposed maglev system was manufactured using the optimization results. Fig. 18 shows the manufactured maglev system. The mover and connection coil covers are made of aluminum. There are three laser interferometers to measure the in-plane position and three gap sensors for out-of-plane.

## 6. Basic Performance

To evaluate basic performance, the stage controlled feedback sensors. The six capacitive sensors are installed at the corner of the stator for the homing process and basic performance evaluation. For feedback control, DS1005 (dSPACE, Germany) is used. The schematic diagram of the hardware setup is shown in Fig. 19.

Fig. 20 shows the in-position stability during levitation. The in-plane position is kept within ±150nm in translational directions and ±0.15 arcsec in a rotational direction. The positioning stability in the x-direction is better than that of the y-direction because the x-direction position is averaged using two sensor signals.

In order to evaluate the minimum positioning resolution, stair trajectory motions were performed. Fig. 21 shows the measurement result of the resolution test. In the translational direction, 100 nm, 340

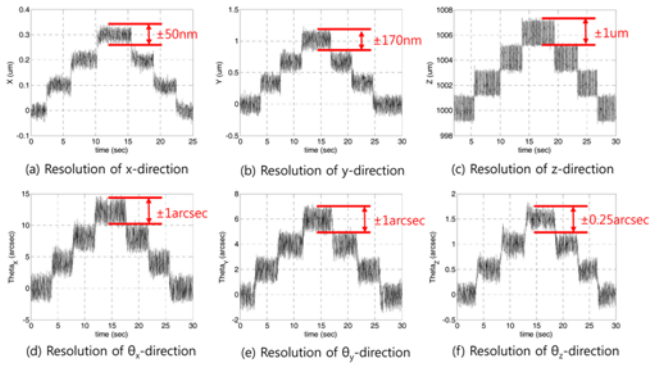


Fig. 21 Minimum position resolution

nm, and 2 um steps are clearly visible in the x, y and z directions. On the whole, in-plane performances are better than out-of-plane performances because the out-of-plane sensors had low resolution. To measure the levitation height, long range capacitive sensors were used.

## 7. Conclusions

In this paper, the long stroke planar motion maglev stage was proposed, optimized, and manufactured. The stator using a copper strip array was proposed for the long stroke. The halbach magnet array was adapted in the designed mover for reinforcing the magnetic flux. We performed magnetic force modeling for the optimization procedure. By using a modal analysis and heat simulation, the stability of the optimized system was checked. The proposed maglev system has a working range of 450 mm and the mover size is larger than 450 mm. Doing so can transfer the 450 mm wafer. Based on the optimal design parameters, the system was manufactured and measured basic performances. In the future, we will examine the entire performance of proposed maglev stage tracking error, maximum velocity, and acceleration. To improve out-of-plane performances, a sensor switch algorithm will be studied in future studies.

## REFERENCES

1. Kim, W. J., Trumper, D. L., and Bryan, J. B., “Linear Motor-Leviated Stage for Photolithography,” CIRP Annals-Manufacturing Technology, Vol. 46, No. 1, pp. 447-450, 1997.
2. Kim, W. J. and Trumper, D. L., “High-Precision Magnetic Levitation Stage for Photolithography,” Precision Engineering, Vol. 22, No. 2, pp. 66-77, 1998.
3. Ueda, Y. and Ohsaki, H., “Fundamental Characteristics of a Small Actuator with a Magnetically Levitated Mover,” Proc. of Power Conversion Conference, pp. 614-621, 2007.
4. Ueda, Y., and Ohsaki, H., “A Planar Actuator with a Small Mover Traveling Over Large Yaw and Translational Displacements,” IEEE Transactions on Magnetics, Vol. 44, No. 5, pp. 609-616, 2008.
5. Ueda, Y. and Ohsaki, H., “Six-Degree-of-Freedom Motion Analysis

of a Planar Actuator with a Magnetically Levitated Mover by Six-Phase Current Controls," IEEE Transactions on Magnetics, Vol. 44, No. 11, pp. 4301-4304, 2008.

6. Jansen, J., Lomonova, E., Vandenput, A., and Compter, J., "Design Tool for a 6-DOF Planar Motor with Moving Permanent Magnets and Standstill Coils," Proc. of 4th International Symposium on Linear Drives for Industry Applications, pp. 8-10, 2003.
7. de Boeij, J., Lomonova, E., and Vandenput, A., "Modeling Ironless Permanent-Magnet Planar Actuator Structures," IEEE Transactions on Magnetics, Vol. 42, No. 8, pp. 2009-2016, 2006.
8. Boeij, J. D. and Lomonova, E., "Experimental Verification of Look-up Table based Real-Time Commutation of 6-DOF Planar Actuators," Journal of System Design and Dynamics, Vol. 3, No. 4, pp. 563-571, 2009.
9. Philips, "Mechatronics and High Precision Engineering," http://www.innovationservices.philips.com/service-catalog/competences/mechatronics-and-high-precision-engineering (Accessed 23 FEB 2015)
10. Jansen, J. W., van Lierop, C. M. M., Lomonova, E. A., and Vandenput, A. J. A., "Ironless Magnetically Levitated Planar Actuator," Journal of Applied Physics, Vol. 103, No. 7, Paper No. 07E905, 2008.
11. Jansen, J. W., Van Lierop, C. M. M., Lomonova, E. A., and Vandenput, A. J. A., "Magnetically Levitated Planar Actuator with Moving Magnets," IEEE Transactions on Industry Applications, Vol. 44, No. 4, pp. 1108-1115, 2008.
12. Lu, X., "6D Direct-Drive Technology for Planar Motion Stages," CIRP Annals-Manufacturing Technology, Vol. 61, No. 1, pp. 359-362, 2012.
13. Furlani, E. P., "Permanent Magnet and Electromechanical Devices," Academic Press, 1st Ed., pp. 97-205, 2001.
14. Akoun, G. and Yonnet, J.-P., "3d Analytical Calculation of the Forces Exerted between Two Cuboidal Magnets," IEEE Transactions on Magnetics, Vol. 20, No. 5, pp. 1962-1964, 1984.
15. Jansen, J. W., Van Lierop, C. M. M., Lomonova, E. A., and Vandenput, A. J. A., "Modeling of Magnetically Levitated Planar Actuators with Moving Magnets," IEEE Transactions on Magnetics, Vol. 43, No. 1, pp. 15-25, 2007.
16. Arora, J. S., "Introduction to Optimum Design," Academic Press, pp. 339-432, 2004.
17. Boender, C. G. E. and Kan, A. R., "Bayesian Stopping Rules for Multistart Global Optimization Methods," Mathematical Programming, Vol. 37, No. 1, pp. 59-80, 1987.